Neuropsychopharmacology (2017) 42, 2072–2086
Official journal of the American College of Neuropsychopharmacology
www.neuropsychopharmacology.org

OPEN

Dysfunction of Microglial STAT3 Alleviates Depressive Behavior via Neuron–Microglia Interactions

Sun-Ho Kwon[1,2,3,9], Jeong-Kyu Han[2,4,5,9], Moonseok Choi[1], Yong-Jin Kwon[1], Sung Joon Kim[4], Eun Hee Yi[6], Jae-Cheon Shin[7], Ik-Hyun Cho[8], Byung-Hak Kim[1,3], Sang Jeong Kim*[,2,3,4,5] and Sang-Kyu Ye*[,1,2,3,6]

[1]Department of Pharmacology, Seoul National University College of Medicine, Seoul, Republic of Korea; [2]Neuro-Immune Information Storage Network Research Center, Seoul National University College of Medicine, Seoul, Republic of Korea; [3]Biomedical Science Project (BK21[PLUS]), Seoul National University College of Medicine, Seoul, Republic of Korea; [4]Department of Physiology, Seoul National University College of Medicine, Seoul, Republic of Korea; [5]Department of Brain and Cognitive Sciences, Seoul National University Graduate School, Seoul, Republic of Korea; [6]Ischemic/Hypoxic Disease Institute, Seoul National University College of Medicine, Seoul, Republic of Korea; [7]Pohang Center for Evaluation of Biomaterials, Pohang, Republic of Korea; [8]Department of Convergence Medical Science, College of Oriental Medicine, Kyung Hee University, Seoul, Republic of Korea

Neuron–microglia interactions have a crucial role in maintaining the neuroimmune system. The balance of neuroimmune system has emerged as an important process in the pathophysiology of depression. However, how neuron–microglia interactions contribute to major depressive disorders has been poorly understood. Herein, we demonstrated that microglia-derived synaptic changes induced antidepressive-like behavior by using microglia-specific signal transducer and activator of transcription 3 (STAT3) knockout (KO) ($STAT3^{fl/fl}$;LysM-$Cre^{+/-}$) mice. We found that microglia-specific STAT3 KO mice showed antidepressive-like behavior in the forced swim, tail suspension, sucrose preference, and open-field tests. Surprisingly, the secretion of macrophage colony-stimulating factor (M-CSF) was increased from neuronal cells in the brains of $STAT3^{fl/fl}$;LysM-$Cre^{+/-}$ mice. Moreover, the phosphorylation of antidepressant-targeting mediators and brain-derived neurotrophic factor expression were increased in the brains of $STAT3^{fl/fl}$;LysM-$Cre^{+/-}$ mice as well as in neuronal cells in response to M-CSF stimulation. Importantly, the miniature excitatory postsynaptic current frequency in the medial prefrontal cortex was increased in $STAT3^{fl/fl}$;LysM-$Cre^{+/-}$ mice and in the M-CSF treatment group. Collectively, microglial STAT3 regulates depression-related behaviors via neuronal M-CSF-mediated synaptic activity, suggesting that inhibition of microglial STAT3 might be a new therapeutic strategy for depression.

Neuropsychopharmacology (2017) **42,** 2072–2086; doi:10.1038/npp.2017.93; published online 7 June 2017

INTRODUCTION

Neuron–microglia interactions have a crucial role in maintaining the neuroimmune system (Rogers *et al*, 2011; Wake *et al*, 2013; Zhan *et al*, 2014). Recent evidence has focused on the imbalance of the neuroimmune system in association with psychiatric disorders, such as major depression (Couch *et al*, 2013). Presumably, microglial dysfunction causes disturbances in synaptic regulation, resulting in major depression. However, the cellular and molecular mechanisms of major depression underpinning the bidirectional interplay between neurons and microglia remain unclear.

*Correspondence: Dr Sang-Kyu Ye, Department of Pharmacology, Seoul National University College of Medicine, Seoul, South Korea. Tel: +82 2 740 8281, Fax: +82 2 745 7996, E-mail: sangkyu@snu.ac.kror Dr Sang Jeong Kim, Department of Physiology, Seoul National University College of Medicine, Seoul, South Korea. Tel: +82 2 740 8229, Fax: +82 2 763 9667, E-mail: sangjkim@snu.ac.kr
[9]These authors contributed equally to this work.
Received 2 December 2016; revised 27 April 2017; accepted 1 May 2017; accepted article preview online 8 May 2017

For decades, many studies focused on novel therapeutic approaches for major depression (Domino *et al*, 2008; Goodyer *et al*, 2007). The intracellular signaling pathways of extracellular signal-regulated kinase (ERK)1/2, Akt and glycogen synthase kinase-3β (GSK3β) have been identified as the potent targets for antidepressants (Duman *et al*, 2016). According to postmortem studies, ERK1/2 signaling, which is downregulated in the brains of patients with major depression (Dwivedi *et al*, 2005; Dwivedi *et al*, 2001), has been implicated in antidepressant treatment (Duman *et al*, 2012b; Einat *et al*, 2003; Tardito *et al*, 2006). Although the blockade of the ERK signaling pathway leads to depression-related behaviors, antidepressant treatments increase ERK phosphorylation (Gourley *et al*, 2007; Hisaoka *et al*, 2007). In addition, GSK3β is regarded as a key factor involved in psychiatric diseases (Beurel *et al*, 2015; Chuang *et al*, 2011; Jope and Roh, 2006). Recent studies showed increased GSK3β activity in the cortical regions of postmortem brains of suicide victims who had suffered from depression (Karege *et al*, 2007). However, the inactivation of GSK3β using lithium or valproate may alleviate unipolar depression (Chen *et al*, 2000; Cipriani *et al*, 2006; Davis *et al*, 1996). GSK3β is

also negatively regulated by phosphatidylinositol 3-kinase-mediated Akt activation (Fang *et al*, 2000).

Despite having a sufficient knowledge of ERK1/2 and Akt/GSK3β signaling pathways, the etiological factors leading to major depression remain unknown. Recent studies showed that neuroinflammation caused by stress-induced activation of microglia leads to depressive-like behaviors (Brites and Fernandes, 2015; Steiner *et al*, 2011; Streit *et al*, 2004). In addition to microglial activation, microglial senescence and decline can negatively affect neurogenesis, causing major depression (Caldeira *et al*, 2014; Kreisel *et al*, 2014). These findings suggest the importance of microglial activation status in depression.

Microglia provide pro- and anti-inflammatory cytokines as mediators for the neuroimmune system. Signal transducer and activator of transcription 3 (STAT3) is one of the transcription factors for cytokine production (El Kasmi *et al*, 2006), such as soluble intracellular cell adhesion molecule-1 (sICAM-1) (Park *et al*, 2013), interleukin (IL)-6 (Mori *et al*, 2011), IL-10 (Riley *et al*, 1999), tumor necrosis factor-α (TNF-α) (Chabot *et al*, 1997; Riazi *et al*, 2008) and IL-1β (Clausen *et al*, 2008). These cytokines have been identified as mediators for the neuroimmune system of depression (Hodes *et al*, 2015). For example, the IL-6/STAT3 signaling pathway was shown to be involved in depressive-like behavior (Kong *et al*, 2015). In addition, pathological levels of these cytokines contribute to behavioral deficits such as depressive-like behavior (Audet and Anisman, 2013; Felger and Lotrich, 2013; Khairova *et al*, 2009; Schiepers *et al*, 2005), requiring a more sophisticated manipulation of cytokine levels.

In this study, we hypothesized that STAT3 signaling in microglia affects neuron–microglia interactions via secreted cytokines, resulting in synaptic and behavioral changes. To investigate the key factors regulated by microglial STAT3 in neuron–microglia interactions, we used microglia-targeted STAT3-deficient mice and analyzed the molecular mechanisms and their behavioral phenotypes. As a result, we revealed that STAT3 dysfunction in microglia led to antidepressive-like behavior via crosstalk between neurons and microglia, suggesting a novel therapeutic avenue for major depression.

MATERIALS AND METHODS

Experimental Animals and Genotyping

Mice homozygous for the loxP-flanked (floxed) *Stat3* gene ($STAT3^{fl/fl}$) were kindly gifted from Dr S Akira. Mice carrying a Cre transgene under the control of the distal LysM promoter (LysM-$Cre^{+/+}$) were purchased from the Jackson Laboratory (Bar Harbor, ME). Mice with a STAT3 deletion in myeloid cells were generated by crossing mice with the floxed STAT3 allele with mice expressing Cre under the control of the LysM promoter. Genomic DNA was isolated from tail tips using a NucleoSpin genomic DNA purification kit (Macherey-Nagel GmbH, Duren, North Rhine-Westphalia, Germany). The PCR reaction was performed using AccuPower PCR premix (Bioneer, Daejeon, Korea) with the primers, which are specific for exons 22 and 23 of STAT3 and Cre transgene, according to the manufacturer's instructions. All experiments were performed with male mice aged 8–10 weeks. Experimental animals were maintained under specific pathogen-free conditions and 22 ± 1 °C with a reversed 12 h light–dark cycle (lights on at 0700 h). All experimental procedures were reviewed and approved by the Institutional Animal Care and Use Committee at the College of Medicine, Seoul National University.

Primary Microglia Cell Culture

Primary microglia cells were isolated from primary mixed glial cells of 2-day-old mice. To obtain mixed glial cells, cerebral cortices were dissected, carefully stripped of their meninges, and dissociated into a single-cell suspension by trituration. Cells were cultured on poly-L-lysine (Sigma-Aldrich, St Louis, MO)-coated 100 mm^2 culture dish in Dulbecco's modified Eagle's medium (DMEM, Hyclone, Logan, UT) containing 10% fetal bovine serum (FBS) and 1% penicillin–streptomycin solution (Gibco, Grand Island, NY), and incubated at 37 °C in 5% CO_2. On the third day of culture, cells were vigorously washed with pipetting and the media was replaced to remove debris. After 6 days *in vitro*, cells were transferred to a T-75 flask and incubated for 1–3 weeks. Then, the conditioned media were replaced with fresh media to achieve complete confluence. To isolate microglia, the T-75 flask was rotated (200 rpm, 37 °C, 5 h) using a temperature-controlled, non-humidified shaker, and then supernatant media containing microglia was centrifuged (215 *g*, 5 min). The microglial pellet was suspended and seeded onto poly-L-lysine-coated 60 mm^2 cover glass-bottom dish (SPL Life Sciences, Pocheon, Korea), and incubated at 37 °C in 5% CO_2.

Cell Culture and Co-Culture Experiments

Mouse microglia cell line BV2 and mouse hippocampal neuronal cell line HT22 (ATCC, Manassas, VA) were cultured in DMEM containing 10% FBS and 1% penicillin–streptomycin solution, and incubated at 37 °C in 5% CO_2. HT22 cells were starved before stimulation for 8 h and then stimulated with macrophage colony-stimulating factor (M-CSF) (40 ng/ml, ProSpec, East Brunswick, NJ) in a time-dependent manner or 24 h. Before the co-culture experiment, BV2 cells were seeded in six-well dishes at 4×10^4 cells/well and transfected with STAT3 siRNAs for 24 h. The cells were washed twice with PBS and then incubated in fresh DMEM containing 10% FBS after transfection. Then, the HT22 cells were cultured on 0.4 μm pore-size Falcon cell culture inserts (Corning, Durham, NC) at 2×10^5 cells/well in DMEM containing 10% FBS and co-cultured with BV2 cells for 24 h. To confirm the effect of macrophages on neurons, HT22 cells were treated with culture medium of RAW264.7 cells with or without STAT3 inhibition for 24 h.

siRNA Transfection

BV2 cells and RAW264.7 cells were cultured in the growth condition to a density of 2×10^5 cells in six-well culture plate. The cells were transfected with the siRNAs using HiperFect transfection reagent (Qiagen, Hilden, Germany) according to the fast-forward protocol of manufacturer's instructions. STAT3 siRNAs targeting two different regions of STAT3 (SI01435287 and SI01435294) and a negative control siRNA (1027280) were purchased from Qiagen.

Immunohistochemistry

Brains of mice were perfused with buffer containing 4% paraformaldehyde, fixed for 2 days in 4% paraformaldehyde at 4 °C, and embedded in paraffin. The paraffin blocks were cut using a microtome (4 μm, Finesse E+, Thermo Shandon, Runcom, UK). Paraffin slices were mounted on the silane-coated micro slides (Muto Pure Chemicals, Tokyo, Japan) and then allowed to air dry at room temperature in the dark for 24 h. Before immunostaining, the slides were deparaffinized in xylene, dehydrated through graded alcohols, and heated in citrate buffer for 10 min. Nonspecific binding was blocked with 5% normal goat serum (Vector Laboratories, Burlingame, CA) in PBS. For immunocytochemistry, cells were grown on a poly-L-lysine-coated 60 mm^2 cover glass-bottom dish for 24 h and rinsed with PBS at room temperature. Then, the cells were fixed with 4% paraformaldehyde for 10 min and permeabilized in 0.1% Triton X-100. Nonspecific binding was blocked with 1% bovine serum albumin (Bovogen, East Keilor, VIC, AUS) in PBS. The fluorescent immunostaining was performed with the primary antibodies for p-STAT3 (1:200, Cell Signaling Technology, MA), STAT3 (1:200, Abcam, Cambridge, UK), Iba-1 (1:200, Wako, Japan), Iba-1 (1:200, Novus Biologicals, CO), and NeuN (1:200, Merck Millipore, MA), and visualized using Cy3 goat anti-mouse IgG, 488 goat anti-mouse IgG, Cy3 donkey anti-rabbit IgG (1:200, BioLegend, CA), 488 donkey anti-rabbit IgG (1:200, Abcam), and 488 bovine anti-goat IgG (1:200, Santa Cruz Biotechnology, CA, USA). The slides were mounted with 4',6-diamidino-2-phenylindole, and images were collected using the LSM510 program on a confocal microscope (Carl Zeiss MicroImaging, München, Germany).

Restraint Stress Procedure

Mice were transferred to a behavior analysis test room before initiating chronic stress procedures. For the chronic stress, the experimental group was immobilized in a rodent restrainer (Ø 30 × 95 mm) and separated from the control group for the duration (2 h a day for 14 consecutive days). After the chronic restraint stress, the mice were returned to their home cages for a day and then behavioral experiments were conducted.

Behavioral Experiments

Behavioral experiments were performed independently according to the behavioral test paradigm and separate groups were used for each behavioral test paradigm. Experimental mice were subjected to tail suspension and forced swimming tests at intervals of 1 day after 14 days of chronic restraint stress to assess despair-based behavior. A separate cohort of mice was used to conduct sucrose preference test to assess reward-based behavior under normal and chronic stress conditions. Another group was used to assess behavior based on anxiety and locomotion; the following series of behavioral experiments were conducted at intervals of 2 days: handling, elevated plus maze test, open-field test, and rotarod test. All mice were killed immediately after the behavioral experiment and all brain tissues of the mice used in the behavioral experiments under chronic restraint stress were extracted.

Forced Swim Test

The forced swim test was performed as described previously (Page *et al*, 1999). Briefly, mice were placed in a glass beaker (2 l beaker), which was filled to a depth of 18 cm with water (25 °C). The water was regularly changed between subjects. The duration of immobility was recorded and measured with a video camera for 6 min.

Tail Suspension Test

Mice were suspended by their tails from a steel bar using adhesive tape in a chamber with opaque walls. The distance between the floor of the chamber and the steel bar was ~ 40 cm. Mice that climbed onto their tails or fell off during the test were excluded from analyses. Mice movements were videotaped for 6 min and the total duration of immobility recorded.

Sucrose Preference Test

The sucrose preference test was conducted as described previously (Strekalova *et al*, 2004). After food and water deprivation for 24 h, mice were given free access to both water and 1% sucrose solution in individual cages for 24 h. The position of each bottle was switched after 12 h to rule out side preference. The consumption of water and sucrose solution was measured by weighing the bottles. The preference for sucrose solution was calculated as a percentage of the volume of consumed sucrose solution over the total volume of liquid drunk.

Open-Field Test

Mice were placed in the center of an open field box (40 × 40 × 40 cm), illuminated by the light of 20 lx intensity,

Figure 1 Targeting signal transducer and activator of transcription 3 (STAT3) in microglia by using $STAT3^{fl/fl}$;LysM-$Cre^{+/-}$ mice. (a) Schematic representation of breeding strategy. The first offspring (F1) were obtained from a $STAT3^{fl/fl}$/LysM-$Cre^{+/+}$ crossing and $STAT3^{wt/fl}$;LysM-$Cre^{+/-}$ (F1) were further mated with STAT3 floxed mice. The second offspring (F2) were divided into four groups: $STAT3^{wt/fl}$;LysM-$Cre^{-/-}$, $STAT3^{fl/fl}$;LysM-$Cre^{-/-}$, $STAT3^{wt/fl}$;LysM-$Cre^{+/-}$, and $STAT3^{fl/fl}$;LysM-$Cre^{+/-}$. (b) PCR analysis of STAT3 floxed ($STAT3^{fl/fl}$), wild-type (WT) ($STAT3^{wt/fl}$) and Cre genes in the second offspring. (c) Immunofluorescence staining for STAT3 (red), Iba-1 (green) and 4',6-diamidino-2-phenylindole (DAPI; blue) was performed in the prefrontal cortex (PFC) of the WT and knockout (KO) mice. Scale bar = 40 μm. Scale bar of the enlarged image = 10 μm. The graph shows intensity profiles illustrating STAT3/Iba-1 co-localization measurements. (d) Immunocytochemistry for STAT3 (green) and Iba-1 (red) was performed in the primary microglia cells of the WT and KO mice. Scale bar = 50 μm. (e) The relative immunofluorescence intensity was used to represent protein levels of STAT3 and Iba-1 (STAT3; 1 ± 0.058 *vs* 0.245 ± 0.021, Iba-1; 1 ± 0.075 *vs* 0.974 ± 0.054 in primary microglia of the WT and KO mice, n = 3 mice/group, respectively). (f) Western blot analysis of STAT3, Iba-1, PSD95, and GFAP in primary microglia, neurons, and astrocytes of the WT and KO mice. Data are means ± SEM, and $*p < 0.05$, $**p < 0.01$, and $***p < 0.001$. Representative data from three independent experiments are shown.

and the mice movements were recorded with a video camera for 30 min. The total distance traveled and time spent in the center of the entire open field (20 × 20 cm) were calculated using video tracking software (EthoVision XT 8.5, Noldus).

Elevated Plus Maze Test

The elevated plus maze consisted of two open arms (30 × 5 cm) and two closed arms of the same size, with 15 cm high side walls. The four arms and central square were

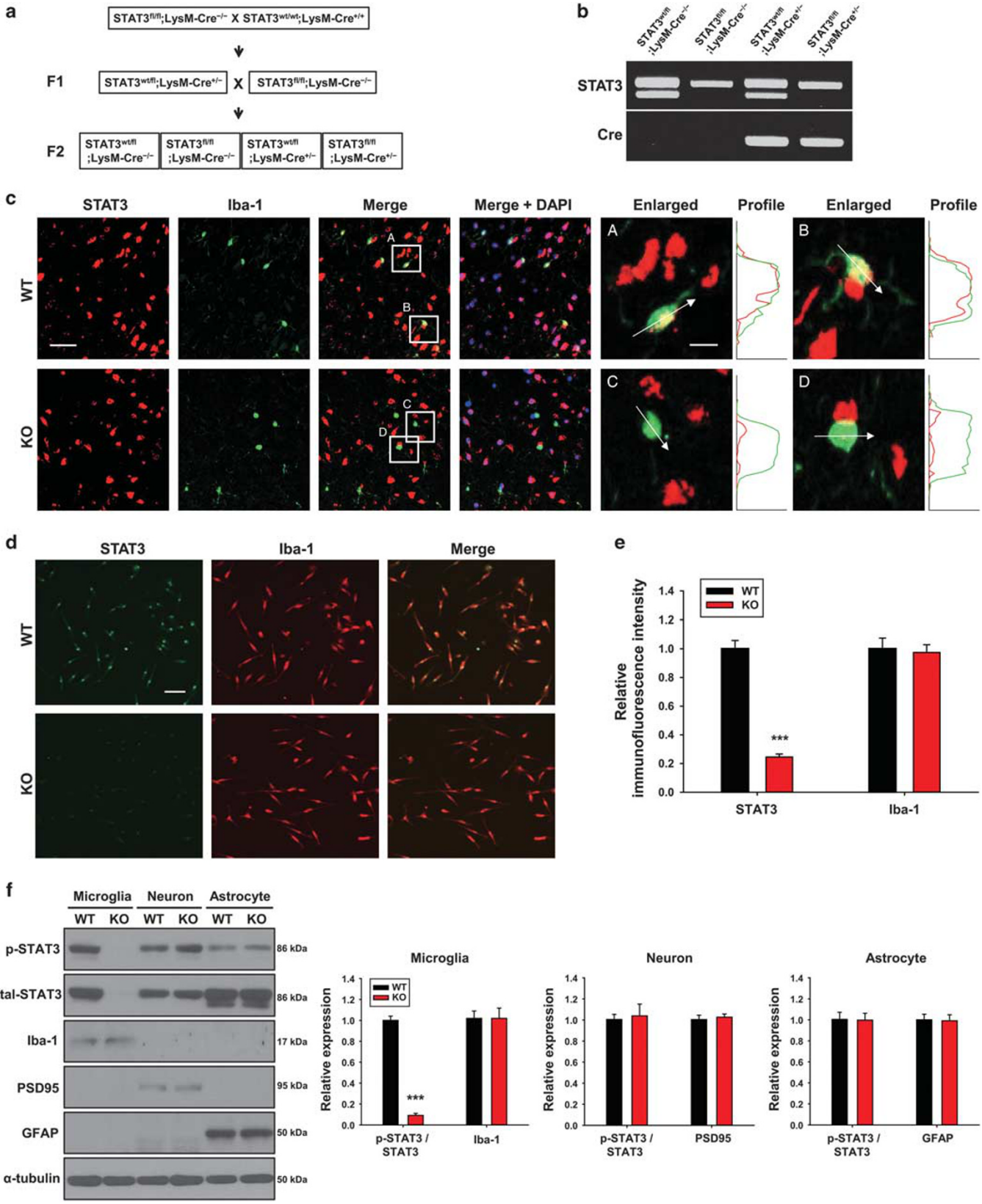

50 cm above the ground. Mice were placed in the central square of the maze (5 × 5 cm), facing the open arms. The mice movements were recorded during a 5 min test period. The number of entries and the time spent in the open and closed arms were calculated using video tracking software (EthoVision XT 8.5, Noldus).

Rotarod Test

The rotarod test was performed by a coordination test system (Rotamex 5, Columbus). The mice were placed on a rotating rod (3 cm in diameter) accelerated from 3 to 50 rpm for 6 min.

Cytokine Array and Enzyme-Linked Immunosorbent Assay (ELISA)

The expression of cytokines and chemokines in the culture supernatant was assessed with a mouse cytokine antibody array panel A (R&D Systems, MN) according to the manufacturer's instructions. Total M-CSF in the conditioned medium of the cultured cells was measured using the quantikine ELISA kit (R&D Systems) according to the manufacturer's instructions. The data were presented as absorbance units at 450 nm and correction absorbance units at 540 nm from three independent experiments.

RNA Isolation and Quantitative Real-Time PCR

Total RNA was isolated from BV2 and HT22 cells using an RNAiso Plus reagent (Takara, Shiga, Japan) and cDNA was synthesized using ReverTra Ace qPCR RT Master Mix (TOYOBO, Osaka, Japan). Quantitative real-time PCR was performed using the EvaGreen qPCR Mastermix (Applied Biological Materials), and the results were normalized to the signals of GAPDH expression. Primers for CCL2 (QT00167832), STAT3 (QT00148750), ICAM-1 (QT00155078), TNF-α (QT00104006), IL-1β (QT01048355), IL-6 (QT00098875), IL-10 (QT00106169), M-CSF (QT01164324), and GAPDH (QT01658692) were purchased from Qiagen.

Western Blotting

Cells were washed with the cold PBS and then lysed in the Triton lysis buffer containing 1% Triton X-100, 50 mM Tris-HCl (pH 7.4), 0.35 M NaCl, 0.5% Nonidet P-40, 10% glycerol, 0.1% SDS, 1 mM EDTA, 1 mM EGTA, 0.2 mM Na_3VO_4, 1 mM PMSF, and 0.5 mM NaF. Brain tissue was homogenized and lysed in the triton lysis buffer. After incubation for 30 min on ice, insoluble debris was removed by centrifugation at 16 000 *g* for 10 min at 4 °C. The lysates were resolved in SDS-polyacrylamide gel electrophoresis and transferred to nitrocellulose membranes (GE Healthcare, Pittsburgh, PA). The membranes were blocked in 5% skim-milk (LPS Solutions, Daejeon, Korea) and probed with the primary antibodies for phospho-STAT3, STAT3, phospho-ERK1/2, ERK1/2, phospho-Akt, Akt (1:1000, Cell Signaling Technology), brain-derived neurotrophic factor (BDNF), phospho-GSK3β, GSK3β (1:1000, Santa Cruz Biotechnology), α-tubulin (1:1000, Thermo Scientific, Grand Island, NY), VGLUT1, PSD95 (1:2000, 1:1000, Synaptic Systems, Göttingen, Germany), Synaptophysin (1:1000, Epitomics, Burlingame, CA), GFAP (DAKO, CA), and Iba-1 (Novus Biologicals) for the target molecules, followed by HRP-conjugated secondary antibodies for goat anti-mouse IgG, goat anti-rabbit IgG (1:10 000, Enzo Life Science, NY), and donkey anti-goat IgG (1:10 000, Santa Cruz Biotechnology). The membranes were visualized using an ECL detection kit (SurModic, Eden Prairie, MN).

Slice Preparation and Electrophysiology

Mice were anesthetized with isoflurane and decapitated, and the brains were immediately removed and placed in ice-cold slicing solution (0–4 °C) containing the following artificial cerebrospinal fluid: 124 mM NaCl, 2.5 mM KCl, 1 mM NaH_2PO_4, 1.3 mM $MgCl_2$, 2.5 mM $CaCl_2$, 26.2 mM $NaHCO_3$, and 20 mM D-glucose, bubbled with a gas mixture of 5% CO_2/95% O_2 to maintain a pH of 7.4. Coronal slices containing medial prefrontal cortex (mPFC) were obtained using a Vibratome (slice thickness 250 μm; Leica VT1200S; Leica, Nussloch, Germany). After cutting, the slices were kept for 30 min at 35 °C and stimulated with M-CSF (10 nM) for synaptosomal preparations and whole-cell recordings. Whole-cell recordings in the mPFC pyramidal cells were performed in the voltage-clamp mode using an amplifier (HEKA Instruments, Lambrecht/Pfalz, Germany). The signal was acquired at 10 kHz and low-pass filtered at 5 kHz. For recording the spontaneous miniature excitatory postsynaptic currents (mEPSCs), the recording electrodes (resistance 2–4 MΩ) were filled with a solution containing (in mM) 135 mM Cs-methane sulfonate, 10 mM CsCl, 10 mM HEPES, 4 mM Mg_2ATP, 0.4 mM Na_3GTP, and 0.2 mM EGTA (pH 7.25). Synaptic responses were analyzed by Mini Analysis Program, Synaptosoft.

Figure 2 Loss of microglial signal transducer and activator of transcription 3 (STAT3) leads to antidepressive-like behavior. (a) Under control or chronic restraint stress conditions, immobility time of the wild-type (WT) and knockout (KO) mice was assessed by tail suspension test (Control; 148.943 ± 9.943 s *vs* 103.537 ± 13.837 s, $n = 12$ and 11, Stress; 198.208 ± 8.490 s *vs* 124.013 ± 13.878 s in the WT and KO mice, $n = 9$ and 10, respectively). (b) Under control or chronic restraint stress conditions, immobility time of the WT and KO mice was assessed by forced swim test (Control; 115.945 ± 9.695 s *vs* 65.678 ± 10.593 s, $n = 10$ and 11, Stress; 197.328 ± 9.733 s *vs* 131.727 ± 16.008 s in the WT and KO mice, $n = 9$ and 10, respectively). (c) Preference for sucrose under control or chronic restraint stress conditions (Control; 75.776 ± 1.914% *vs* 77.061 ± 1.943%, Stress; 55.13 ± 4.146% *vs* 75.833 ± 2.341% in the WT and KO mice, $n = 10$ and 9, respectively). (d) Total liquid intake under control or chronic restraint stress conditions (Control; 4.91 ± 0.119 ml *vs* 4.95 ± 0.092 ml, Stress; 5.24 ± 0.121 ml *vs* 5.1 ± 0.097 ml in the WT and KO mice, $n = 10$ and 9, respectively). (e) Total distance (11794.746 ± 811.651 cm *vs* 9267.810 ± 819.674 cm in the WT and KO mice) and (f) time spent in the center of the open field (160.3 ± 19.6 s *vs* 168.9 ± 34 s in the WT and KO mice, $n = 8$ and 9, respectively). (g) Time spent in the open arms of plus arms (133.6 ± 17.5 s *vs* 150.4 ± 30.2 s in the WT and KO mice, $n = 8$ and 9, respectively). (h) Total running time on the rotating drum ($n = 8$ and 9, respectively). Data are means ± SEM, $^{*}p < 0.05$, $^{**}p < 0.01$, and $^{***}p < 0.001$ compared with WT; $^{\#}p < 0.05$, $^{\#\#}p < 0.01$, and $^{\#\#\#}p < 0.001$ compared with control.

Golgi Staining

Dendritic spine density was analyzed using an FD Rapid GolgiStain Kit (FD Neurotechnologies, Baltimore, MD) was used according to the manufacturer's instructions. In brief, mice were anesthetized with isoflurane and decapitated. The brains were immediately removed, rinsed, and immersed in the impregnation solution, and stored at room temperature for 2 weeks in the dark. The brains were transferred into a solution containing sucrose and stored at room temperature in the dark for at least 3 days. Frozen slices of the brain were cut using a freezing microtome (100 μm, Cryotome FE,

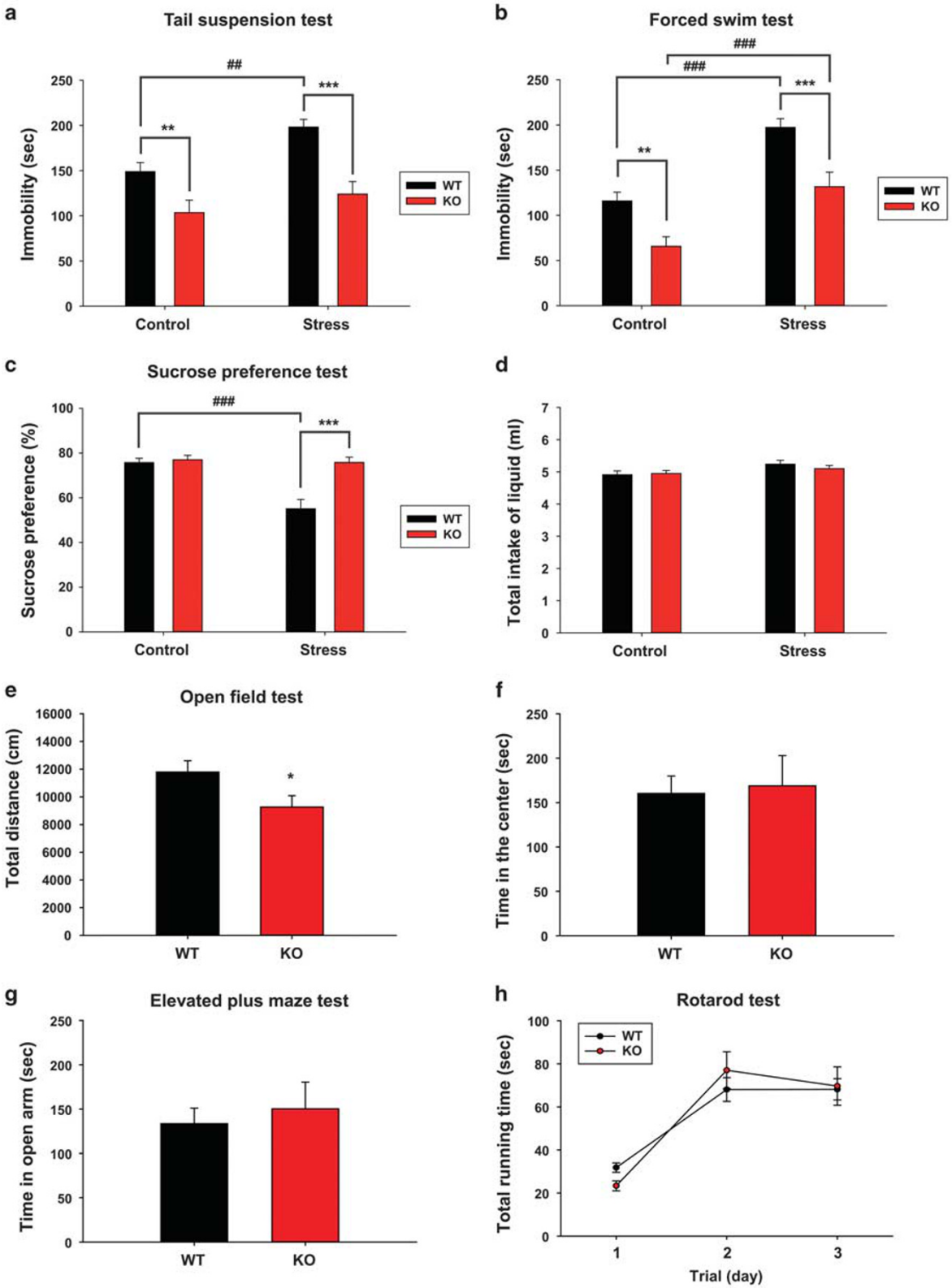

Thermo Shandon). The slices were mounted on gelatin-coated microscope slides and then allowed to air dry at room temperature in the dark for 3 days. Slides were then rinsed with distilled water before being dehydrated in absolute alcohol, cleared with xylene, and covered with non-acidic synthetic balsam and cover slips.

Brain Synaptosomal Preparation

Brain synaptosomal preparation was performed as described previously (Kamat *et al*, 2014). In brief, the prefrontal cortex was homogenized in 10% (w/v) of 0.32 M sucrose-HEPES buffer on ice and the homogenate was centrifuged at 600 *g* for 10 min at 4–8 °C. The HEPES buffer was composed of 145 mM NaCl, 5 mM KCl, 2 mM $CaCl_2$, 1 mM $MgCl_2$, 5 mM glucose, and 5 mM HEPES (pH 7.4). The supernatant was diluted 1:1 with 1.3 M HEPES sucrose, to yield a suspension with a final concentration of 0.8 M HEPES sucrose. This suspension was further centrifuged at three times with HEPES buffer at 12 000 *g* for 15 min at 4 °C. The pellet consisting of synaptosomes was suspended in RIPA buffer (mixed with a protease inhibitor and PMSF) along with 0.2% TritonX-100 and centrifuged at 20 000 *g* for 30 min. The resulting synaptosomes were immediately used for the western blotting.

Statistical Analysis

One-way analysis of variance (ANOVA) was used for the statistical analysis of cytokine array. Multiple comparisons were investigated *via* Tukey-Kramer's *post hoc* test. Two-way ANOVA (genotype × stress) was applied to assess behavioral experiments with chronic restraint stress. Bonferroni's *post hoc* test was performed if applicable. Repeated-measures ANOVA (genotype × trial session) was used to analyze locomotive activity, and learning and memory. Group comparisons of immunofluorescence intensity, RNA and protein expressions, and electrophysiology data were performed by Student's *t*-tests. The data were assessed to ensure normality with the Shapiro–Wilk test, and where violations of the normality assumptions were found, non-parametric statistics were conducted. All data are presented in means ± SEM. All statistical analyses were conducted using SigmaPlot software (ver. 13, Systat Software, San Jose, CA).

RESULTS

Targeting STAT3 in Microglia by Using $STAT3^{fl/fl}$;LysM-$Cre^{+/-}$ Mice

Microglia are unique glial cells derived from common myeloid progenitors during developmental stages of the CNS, possibly explaining the experimental paradigm for neuron-microglia interactions. In this study, we targeted STAT3 in microglia, a key transcription factor for immune responses, due to its relevance in the regulation of cytokine expression levels. We employed the myeloid cell-specific STAT3-deficient mouse model by breeding STAT3 floxed mice and LysM-Cre mice. We denoted $STAT3^{wt/fl}$;LysM-$Cre^{+/-}$ as wild-type (WT) and $STAT3^{fl/fl}$;LysM-$Cre^{+/-}$ as KO (Figure 1a; see Materials and Methods).

To verify a STAT3 depletion in microglia, *STAT3* gene KO was first confirmed by genotyping (Figure 1b). The absence of microglial STAT3 expression (red, anti-STAT3; green, anti-Iba-1) in the prefrontal cortex of $STAT3^{fl/fl}$;LysM-$Cre^{+/-}$ mice was verified using tissue immunostaining. The profile of immunofluorescence intensity showed that STAT3 was not expressed in microglia (Figure 1c). In primary cultured microglial cells (red, anti-Iba-1) obtained from the STAT3-deficient mouse model, the expression of STAT3 (green, anti-STAT3) was completely depleted in $STAT3^{fl/fl}$;LysM-$Cre^{+/-}$ mice, as well as shown in quantitative data (Figures 1d and e; $p<0.001$). From the immunoblotting analysis, we also confirmed that the STAT3 expression was depleted specifically in microglia, but not in neurons and astrocytes that were isolated from each primary cultured cell (Figure 1f; $p<0.001$). In addition, depletion of STAT3 in microglia had no effect on the expression of STAT3 in neurons and on the number of both neurons and microglia in $STAT3^{fl/fl}$;LysM-$Cre^{+/-}$ mice (Supplementary Figure S1).

Loss of Microglial STAT3 Leads to Antidepressive-Like Behavior

To investigate the behavioral correlates of neuron–microglia interactions, we examined mood-related behaviors in the model mice. Interestingly, we observed antidepressive-like behaviors in the tail suspension test, forced swim test, sucrose preference test, and open-field test. As animal models of stress-induced depression to validate the stress-resistant behavior, we induced chronic restraint stress for 2 h a day for 2 weeks. The level of STAT3 phosphorylation were increased in the WT, but not in $STAT3^{fl/fl}$;LysM-$Cre^{+/-}$ mice under chronic stress conditions (Supplementary Figure S2). In the tail suspension and forced swim tests, the immobility time was significantly reduced in $STAT3^{fl/fl}$;LysM-$Cre^{+/-}$ mice both in control and in chronic stress conditions (Figure 2a; genotype × stress interaction: $F_{(1,38)}=1.443$, $p=0.237$; genotype effect: $F_{(1,38)}=24.906$, $p<0.001$; stress effect: $F_{(1,38)}=8.469$, $p=0.006$, and Figure 2b; genotype × stress interaction: $F_{(1,36)}=0.415$, $p=0.523$; genotype effect: $F_{(1,36)}=23.718$, $p<0.001$; stress effect: $F_{(1,36)}=38.4$,

Figure 3 Downregulation of microglial signal transducer and activator of transcription 3 (STAT3) increases neuronal macrophage colony-stimulating factor (M-CSF) levels in neuron-microglia interactions. (a) Expression of cytokines and chemokines in the whole brain of the wild-type (WT) and knockout (KO) mice using cytokine arrays. (b) The bar graph was calculated for each cytokine with mean pixel density. (c) Relative mRNA levels of M-CSF, intracellular cell adhesion molecule-1 (ICAM-1), interleukin (IL)-1β and tumor necrosis factor (TNF)-α in the prefrontal cortex, (d) cerebellum, and (e) hippocampus. (f) Expression of cytokines and chemokines in the peritoneal macrophages of the WT and KO mice using cytokine arrays. (g) The bar graph was calculated for each cytokine with men pixel density. (h) Schematic representation of the co-culture system between BV2 and HT22 cells. (i) Relative mRNA levels of STAT3, M-CSF, ICAM-1, IL-1β, and TNF-α in BV2 cells, and (j) HT22 cells from the co-culture system was quantified by qRT-PCR. (k) Concentration of M-CSF from the co-cultured medium (217 ± 3.4 pg/ml *vs* 300 ± 9 pg/ml, n = 8/group, respectively) and (l) the BV2-cultured medium (29.2 ± 2.6 pg/ml *vs* 26.7 ± 2.2 pg/ml, n = 3/group, respectively) were determined by enzyme-linked immunosorbent assay (ELISA). The whole cytokine array panels are presented in Supplementary Figure S10. Data are means ± SEM and $*p<0.05$, $**p<0.01$, and $***p<0.001$. Representative data from three independent experiments are shown.

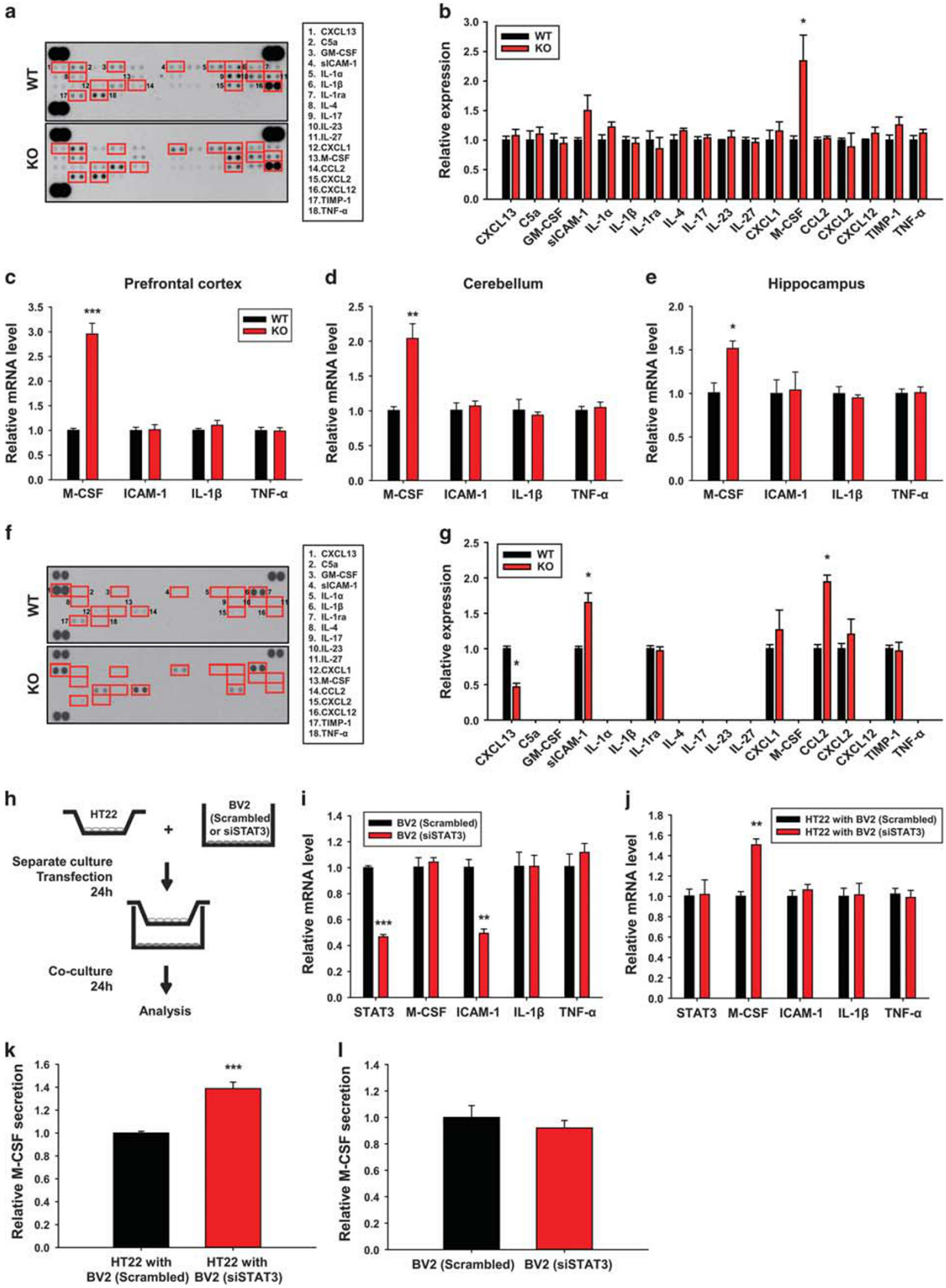
a
WT
KO
1. CXCL13
2. C5a
3. GM-CSF
4. sICAM-1
5. IL-1α
6. IL-1β
7. IL-1ra
8. IL-4
9. IL-17
10.IL-23
11.IL-27
12.CXCL1
13.M-CSF
14.CCL2
15.CXCL2
16.CXCL12
17.TIMP-1
18.TNF-α
b
Relative expression
WT
KO
CXCL13 C5a GM-CSF sICAM-1 IL-1α IL-1β IL-1ra IL-4 IL-17 IL-23 IL-27 CXCL1 M-CSF CCL2 CXCL2 CXCL12 TIMP-1 TNF-α
c
Prefrontal cortex
Relative mRNA level
M-CSF ICAM-1 IL-1β TNF-α
d
Cerebellum
e
Hippocampus
f
g
h
HT22
BV2 (Scrambled or siSTAT3)
Separate culture
Transfection 24h
Co-culture 24h
Analysis
i
BV2 (Scrambled)
BV2 (siSTAT3)
STAT3 M-CSF ICAM-1 IL-1β TNF-α
j
HT22 with BV2 (Scrambled)
HT22 with BV2 (siSTAT3)
k
Relative M-CSF secretion
HT22 with BV2 (Scrambled)
HT22 with BV2 (siSTAT3)
l
BV2 (Scrambled)
BV2 (siSTAT3)

$p<0.001$). Under chronic stress conditions, the immobility time of STAT3$^{fl/fl}$;LysM-Cre$^{+/-}$ mice was increased in the forced swim tests, but not in the tail suspension tests (Figure 2b). These results indicate that STAT3$^{fl/fl}$;LysM-Cre$^{+/-}$ mice had intrinsic resistance owing to genetic modification and showed partial resilience to chronic stress conditions. To ensure consistency among WT groups, immobility time was further compared in the tail suspension and forced swim test. The WT groups did not differ from each other (Supplementary Figure S3). Corroborating the generality of these findings, the WT mice subject to chronic restraint stress exhibited a significant decrease in sucrose preference. However, the sucrose preference of STAT3$^{fl/fl}$;LysM-Cre$^{+/-}$ mice was higher than WT mice under chronic stress conditions (Figure 2c; genotype × stress interaction: $F_{(1,35)}=12.295$, $p=0.001$; genotype effect: $F_{(1,35)}=15.764$, $p<0.001$; stress effect: $F_{(1,35)}=15.601$, $p<0.001$). Both WT and STAT3$^{fl/fl}$;LysM-Cre$^{+/-}$ mice showed similar amounts of liquid intake under both control and stressed conditions (Figure 2d; genotype × stress interaction: $F_{(1,35)}=0.573$, $p=0.454$; genotype effect: $F_{(1,35)}=0.177$, $p=0.677$; stress effect: $F_{(1,35)}=4.071$, $p=0.051$). Lastly, we verified reduced locomotor activity of STAT3$^{fl/fl}$;LysM-Cre$^{+/-}$ mice in the open-field test (Figure 2e; $p<0.05$), but not the exploration time in the center area (Figure 2f). A previous study demonstrated that the stressed mice showed enhanced locomotor activity under the light of modest brightness (Strekalova *et al*, 2004). Our results suggest that antidepressive-like behavior was observed in STAT3$^{fl/fl}$;LysM-Cre$^{+/-}$ mice. Collectively, dysregulation of STAT3 in microglia successfully alleviated depressive and stress-induced behaviors.

In addition, we found no differences in body weight, anxiety-related, and motor behaviors of STAT3$^{fl/fl}$;LysM-Cre$^{+/-}$ mice (Supplementary Figure S4a and Figures 2g and h; trial session effect: $F_{(2,30)}=83.245$, $p<0.001$; genotype effect: $F_{(1,15)}=0.008$, $p=0.931$), demonstrating that deletion of STAT3 in microglia had solely contributed to antidepressive effects. We also tested whether the antidepressive effects could affect other cognitive functions associated with learning and memory, but found neither cognitive impairment nor enhancement in STAT3 $^{fl/fl}$;LysM-Cre$^{+/-}$ mice (Supplementary Figure S4b–f).

Downregulation of Microglial STAT3 Increases Neuronal M-CSF Levels in Neuron-Microglia Interactions

To identify key factors affecting antidepressive-like behavior caused by depletion of microglial STAT3, we first examined the cytokine levels in the brain tissue of both WT and STAT3$^{fl/fl}$;LysM-Cre$^{+/-}$ mice using a cytokine array. The data showed that M-CSF was increased solely in STAT3$^{fl/fl}$;LysM-Cre$^{+/-}$ mice (Figures 3a and b; one-way ANOVA: $F_{(1,4)}=9.304$, $p<0.05$). The effect of M-CSF in association with antidepressive-like behavior was highly localized to several brain regions, such as prefrontal cortex, cerebellum, and hippocampus, where M-CSF receptors were primarily expressed (Figure 3c; $p<0.001$, Figure 3d; $p<0.01$, and Figure 3e; $p<0.05$). However, we could not detect any change in the levels of canonical cytokines, such as ICAM-1, IL-1β, TNF-α, IL-6, and IL-10 (Figure 3b and Supplementary Figure S5). These results suggest that M-CSF may be a key factor for regulating antidepressive-like behavior. To determine whether peripheral macrophages had an effect on increasing M-CSF, we applied the same cytokine array to peritoneal macrophages isolated from both WT and STAT3$^{fl/fl}$;LysM-Cre$^{+/-}$ mice (Figure 3f and Supplementary Figure S6a). sICAM-1 and CCL2 were increased, but CXCL13 was decreased in macrophages of STAT3$^{fl/fl}$;LysM-Cre$^{+/-}$ mice (Figure 3g; CXCL13: $F_{(1,2)}=71.092$, $p<0.05$; sICAM-1: $F_{(1,2)}=22.346$, $p<0.05$; CCL2: $F_{(1,2)}=71.906$, $p<0.05$). These factors were expressed at the similar level in the brain tissue, indicating that M-CSF-mediated antidepressive-like behavior was not associated with peripheral macrophages. In short, the results indicate that M-CSF production regulates antidepressive-like behaviors through neuron–microglia interactions.

To mimic the neuron–microglia interactions of STAT3$^{fl/fl}$;LysM-Cre$^{+/-}$ mouse model, we performed *in vitro* co-culture using transwell inserts with both the neuronal cell line HT22 and the microglia cell line BV2 (Figure 3h). Endogenous STAT3 level was silenced by transfection with specific small interfering RNA for STAT3 (siSTAT3) in BV2 cells with the maintenance of cell viability (Supplementary Figure S6b and c). Although the mRNA level of STAT3 and ICAM-1 in BV2 cells decreased in the co-culture system, the M-CSF, IL-1β, and TNF-α levels remained unchanged in the cells (Figure 3i; STAT3: $p<0.001$, ICAM-1: $p<0.01$). Importantly, the mRNA level of M-CSF increased in HT22 cells co-cultured with STAT3 knocked-down BV2 cells, but no change was observed in the STAT3, ICAM-1, IL-1β, and TNF-α mRNA levels (Figure 3j; $p<0.01$).

Based on the results, we hypothesized that the secretion of M-CSF may occur mainly in neuronal cells. To examine this, we measured the concentration of M-CSF using an ELISA in the co-culture system. The amount of secreted M-CSF was highly increased in the co-culture medium of HT22 cells with STAT3-silenced BV2 cells (Figure 3k; $p<0.001$); however,

Figure 4 Macrophage colony-stimulating factor (M-CSF) upregulates antidepressant signaling pathways and brain-derived neurotrophic factor (BDNF) expression. (a) Western blot analysis of BDNF, extracellular signal-regulated kinase (ERK) 1/2, Akt, and glycogen synthase kinase-3β (GSK3β) in the prefrontal cortex (PFC, ctx), cerebellum (ceb), and hippocampus (hip) of the wild-type (WT) and knockout (KO) mice. (b) Western blot analysis of BDNF, ERK1/2, Akt, GSK3β, synaptophysin, PSD95, VGLUT1, GFAP, and Iba-1 in the synaptosomes isolated from the PFC of the WT and KO mice. (c) Western blot analysis of ERK1/2, Akt, GSK3β, synaptophysin, PSD95, VGLUT1, GFAP and Iba-1 in the synaptosomes isolated from PFC slices of the WT mice after a time-dependent M-CSF stimulation (10 nM). (d) Western blot analysis of BDNF, ERK1/2, Akt, and GSK3β in BV2 and HT22 cells from the co-culture set. (e) Western blot analysis of BDNF, ERK1/2, Akt, and GSK3β in HT22 cells after M-CSF stimulation (40 ng/ml) for 24 h. (f) Western blot analysis of ERK1/2, Akt, and GSK3β in HT22 cells after a time-dependent M-CSF (40 ng/ml) stimulation. (g) Western blot analysis of BDNF, ERK1/2, Akt, and GSK3β in HT22 cells treated with RAW264.7 cultured medium with or without STAT3 inhibition. Each quantification of western blotting was obtained with relative densitometry and normalized with α-tubulin. Whole western blotting images of BDNF are presented in Supplementary Figure S11. Data are means ± SEM and $*p<0.05$, $**p<0.01$, and $***p<0.001$. Representative data from three independent experiments are shown.

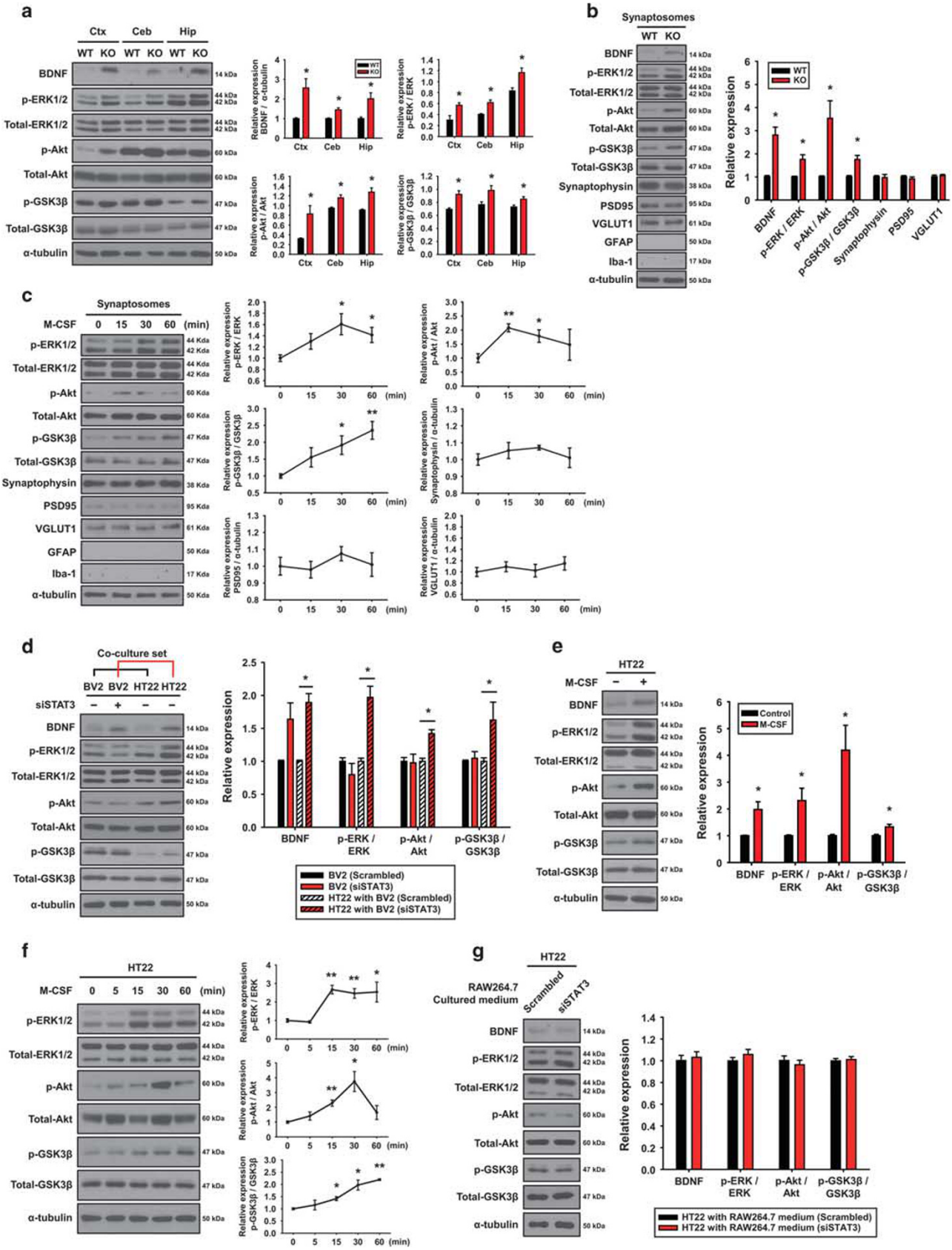
a
Ctx
Ceb
Hip
WT KO WT KO WT KO
BDNF
p-ERK1/2
Total-ERK1/2
p-Akt
Total-Akt
p-GSK3β
Total-GSK3β
α-tubulin
Relative expression BDNF / α-tubulin
Relative expression p-ERK / ERK
Relative expression p-Akt / Akt
Relative expression p-GSK3β / GSK3β
b
Synaptosomes
WT KO
Synaptophysin
PSD95
VGLUT1
GFAP
Iba-1
Relative expression
c
M-CSF 0 15 30 60 (min)
Relative expression PSD95 / α-tubulin
Relative expression VGLUT1 / α-tubulin
d
Co-culture set
BV2 BV2 HT22 HT22
siSTAT3
BV2 (Scrambled)
BV2 (siSTAT3)
HT22 with BV2 (Scrambled)
HT22 with BV2 (siSTAT3)
e
HT22
M-CSF
Control
M-CSF
f
HT22
M-CSF 0 5 15 30 60 (min)
g
HT22
RAW264.7 Cultured medium
Scrambled
siSTAT3
HT22 with RAW264.7 medium (Scrambled)
HT22 with RAW264.7 medium (siSTAT3)

that of M-CSF secretion had no difference between the control and STAT3-silenced BV2 cells (Figure 3l). Thus, the data suggest that ablation of STAT3 in microglia is crucial for the increase in M-CSF production in neuronal cells and that these mechanisms may have a crucial role in neuronal functions, leading to the antidepressive-like behavior in $STAT3^{fl/fl}$;LysM-$Cre^{+/-}$ mice.

M-CSF Upregulates Antidepressant Signaling Pathways and BDNF Expression

To identify how the secreted M-CSF triggers the activation of antidepressant signaling pathways, we investigated BDNF levels and signaling cascades of ERK1/2 and Akt/GSK3β in the $STAT3^{fl/fl}$;LysM-$Cre^{+/-}$ mouse model. We observed that the BDNF expression as well as ERK1/2 and Akt/GSK3β phosphorylation were increased in several brain regions of $STAT3^{fl/fl}$;LysM-$Cre^{+/-}$ mice, including the prefrontal cortex, cerebellum, and hippocampus (Figure 4a; all $p<0.05$). In synaptosomes from the prefrontal cortex of $STAT3^{fl/fl}$;LysM-$Cre^{+/-}$ mice, the phosphorylation of ERK1/2 and Akt/GSK3β was enhanced, along with increased BDNF expression; however, we found no changes in the levels of pre-/post-synaptic proteins, such as synaptophysin, VGLUT1, and PSD95 (Figure 4b; all $p<0.05$). Lastly, we verified the direct effects of M-CSF on ERK1/2 and Akt/GSK3β signaling pathways in a time-dependent manner in synaptosomes from cortical slices of the WT mice. M-CSF stimulation gradually increased phosphorylation of ERK1/2 and Akt/GSK3β in synaptic level (Figure 4c; ERK1/2 at 30, 60 min, Akt and GSK3β at 30 min: $p<0.05$, Akt at 15 min and GSK3β at 60 min: $p<0.01$). The results imply that M-CSF activates antidepressant pathways, along with BDNF production.

We further confirmed the results in *in vitro* co-culture system. The expression of BDNF as well as phosphorylation of ERK1/2 and Akt/GSK3β was increased only in HT22 cells co-cultured with STAT3-silenced BV2 cells (Figure 4d; all $p<0.05$). As expected, BDNF expression was persistently increased and both ERK1/2 and Akt/GSK3β remained phosphorylated after M-CSF stimulation for 24 h in HT22 cells (Figure 4e; all $p<0.05$). Finally, we observed the direct effects of M-CSF within an hour on ERK1/2 and Akt/GSK3β signaling pathways in HT22 cells (Figure 4f; ERK1/2 at 60 min, Akt at 30 min, and GSK3β at 15, 30 min: $p<0.05$, ERK1/2 at 15, 30 min, Akt at 15 min, and GSK3β at 60 min: $p<0.01$). However, we found no direct effects of peritoneal macrophages on neuronal cells. ERK1/2 and Akt/GSK3β signaling pathways did not induce any change in HT22 cells with macrophage cell line RAW264.7 medium regardless of whether STAT3 was downregulated or not (Figure 4g and Supplementary Figure S6d and e). We reasoned that the effects of M-CSF stimulation on microglia should be tested since M-CSF was one of the well-known inducers for intracellular signaling in microglia (Imai and Kohsaka, 2002). Data showed that the phosphorylation of ERK1/2 and Akt/GSK3β did not increase in STAT3-silenced BV2 cells (Supplementary Figure S7). Collectively, our data strongly indicate that M-CSF may be critically involved in antidepressive-like behavior by upregulating BDNF expression through a direct effect on the ERK1/2 and Akt/GSK3β signaling cascades.

Depletion of Microglial STAT3 Enhances M-CSF-Mediated Glutamatergic Neurotransmission

As neuronal mechanisms of depression, the increased synaptic transmission could be a potent mechanism from a therapeutic point of view (Duman and Aghajanian, 2012a). To explore the microglia-derived effects on neurotransmission, we investigated the excitatory synapses of the pyramidal cells (layer 5) in the mPFC by recording α-amino-3-hydroxy-5-methyl-4-isoxazolepropionic acid (AMPA) receptor-mediated mEPSCs. As the representative traces demonstrated (Figure 5a), the cumulative probability distributions of the mEPSC frequency increased in $STAT3^{fl/fl}$;LysM-$Cre^{+/-}$ model mice (Figure 5b; $p<0.05$); however, those of the mEPSC amplitudes were not statistically different (Figure 5c). These results imply that microglia-derived effects could facilitate the release of neurotransmitters on presynaptic synapses.

The above results led us to further investigate whether M-CSF could affect the release of neurotransmitters on presynaptic synapses. We incubated brain slices with M-CSF for 10 min and measured the mEPSCs. As the representative traces illustrated (Figure 5d), the cumulative probability distributions of the mEPSC frequency were increased in the presence of M-CSF (Figure 5e; $p<0.05$); however, those of the mEPSC amplitudes were not statistically different (Figure 5f).

Furthermore, we investigated whether the increase in the mEPSC frequency caused by M-CSF was involved in the presynaptic effect. By stimulating the layer 2/3 of the mPFC, we measured the paired-pulse ratio in the excitatory synapses of the pyramidal cells (layer 5). As the representative traces illustrated (Figure 5g), the probability of neurotransmitter release was increased in $STAT3^{fl/fl}$;LysM-$Cre^{+/-}$ mice (Figures 5h and i; all $p<0.01$). In addition, we analyzed the shape of individual traces of AMPA receptor-mediated EPSCs, but found no differences in decay time and 10%–90% rise time in both $STAT3^{fl/fl}$;LysM-$Cre^{+/-}$ model mice and M-CSF treatment group (Supplementary Figure S8). In morphological perspectives, Golgi staining showed no differences in the number of dendritic spines between the WT and $STAT3^{fl/fl}$;LysM-$Cre^{+/-}$ mice (Figures 5j and k). We concluded that elevated M-CSF secretion in neuronal cells caused by interaction with STAT3-deficient microglia presynaptically enhanced glutamatergic neurotransmission.

DISCUSSION

In the present study, we explored the mechanisms of neuron–microglia interactions. Primarily, we used a microglia-targeted STAT3-deficient mouse model. From an immunological perspective, STAT3 signaling has a major role in immune responses and microglia are CNS-resident immune cells that sense stress in the microenvironment. However, microglia were shown to modulate synaptic activity through functional changes (Wake *et al*, 2013). In the current study, we demonstrated that dysfunction of STAT3 in microglia enhanced M-CSF action on neural

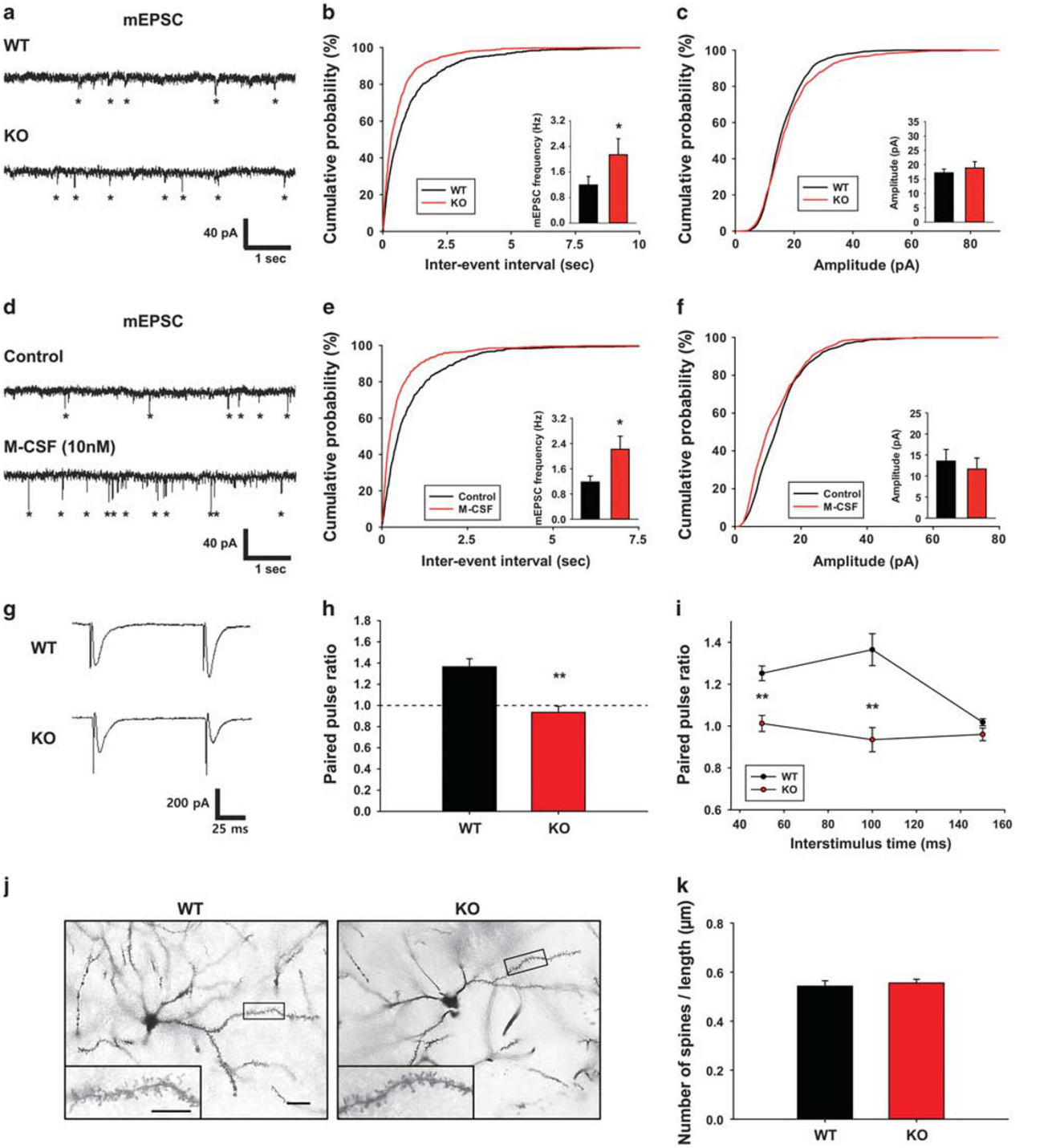

Figure 5 Depletion of microglial signal transducer and activator of transcription 3 (STAT3) enhances macrophage colony-stimulating factor (M-CSF)-mediated glutamatergic neurotransmission. (a) Representative traces of the miniature excitatory postsynaptic currents (mEPSCs) in the wild-type (WT) and knockout (KO) groups ($n = 10$ and 9 neurons/group). Each asterisk indicates synaptic events. (b) Graphs for the cumulative probability of the mEPSC frequency; bar graphs for an average of frequency (1.2 ± 0.27 Hz *vs* 2.14 ± 0.5 Hz in the WT and KO mice, respectively). (c) Graphs for the cumulative probability of the mEPSC amplitudes; bar graphs for an average of amplitudes (17.185 ± 1.306 pA *vs* 18.846 ± 2.186 pA in the WT and KO mice, respectively). (d) Representative traces of the mEPSCs in the control and the M-CSF treatment groups ($n = 6$ neurons/group). (e) Graphs for the cumulative probability of the mEPSC frequency; bar graphs for an average of frequency (1.18 ± 0.19 Hz *vs* 2.22 ± 0.412 Hz in the control and M-CSF treatment groups, respectively). (f) graphs for the cumulative probability of the mEPSC amplitudes; bar graphs for an average of amplitudes (13.538 ± 2.765 pA *vs* 11.651 ± 2.620 pA in the control and M-CSF treatment groups, respectively). (g) Representative traces for paired pulse ratio measurement in WT and KO mice ($n = 6$ and 5 neurons/group). (h) The graph for paired pulse ratio at the 100 ms intervals (paired-pulse ratio (PPR): the ratio of EPSC2/EPSC1) (1.365 ± 0.076 *vs* 0.935 ± 0.058 in the WT and KO mice, respectively). (i) Dependence of PPR on interstimulus intervals at the 50, 100 and 150 ms (1.252 ± 0.035 *vs* 1.013 ± 0.038 at 50 ms, 1.365 ± 0.076 *vs* 0.935 ± 0.058 at 100 ms, 1.018 ± 0.017 *vs* 0.96 ± 0.03 at 150 ms in the WT and KO mice, respectively). (j) Representative images of Golgi staining in the WT and KO groups (n = 5 mice/group). (k) Quantitative data for the number of dendritic spines (0.543 ± 0.022 μm *vs* 0.556 ± 0.015 μm in the WT and KO mice, n = 17 and 23 neurons/group, respectively). Scale bar = 40 μm. Scale bar of the enlarged image = 20 μm. Data are means ± SEM and $*p < 0.05$, $**p < 0.01$, and $***p < 0.001$.

functions along with upregulation of BDNF expression through antidepressant pathways and consequently alleviated depression-related behaviors. These findings could aid in the development of novel pharmaceutical antidepressant drugs.

Our findings on the behavioral association of neuron–microglia interactions show that the STAT3 pathway in microglia may be strongly associated with antidepressive-like behavior. These behavioral experimental results could be categorized as the positive valence system according to Research Domain Criteria for emotional behavior. Despair-based behavior represented by tail suspension and forced swim tests was responsible for willingness to overcome stressful responses, by measuring motility. Similarly, behavioral processes related to hedonic responses were examined in the sucrose preference test for probing the neural systems for reward seeking behavior. Each experimental design may demonstrate partial aspects of depressive symptoms mimicking human patients' behavior; however, it is quite plausible for newly built criteria on human mental researches.

For many decades, accumulating evidence has reported a positive relationship between depression and cytokines and/or chemokines, such as TNF-α, IL-1, IL-6, and the CC chemokine ligand (CCL) family (Khairova *et al*, 2009). A recent study suggested that manipulation of the microglia activation status with microglial stimulators, such as lipopolysaccharide and M-CSF, could be a potent etiological therapeutics for depression symptomatology (Kreisel *et al*, 2014). For example, M-CSF could reduce the depressive-like behavior by activating microglia status under chronic stress conditions. In our microglial STAT3-deficient model, the microglial STAT3 as a sensor of the cytokine profiles was effectively depleted. Notably, the expression of M-CSF was increased in the brains of $STAT3^{fl/fl}$;$LysM\text{-}Cre^{+/-}$ mice. The elevated mRNA levels and the secretion of M-CSF were detected in neuronal cells in *in vitro* co-culture system. These results implied the novel actions of M-CSF in the absence of microglial STAT3. Under altered circumstances by deletion of microglial STAT3, M-CSF can be synthesized in neuronal cells and at the same time affect the neuronal cells themselves. For example, M-CSF is produced with an autocrine/paracrine mechanism of action in distinct brain regions, including the dorsal forebrain, and cerebellum, and has an essential role in neural progenitor cell maintenance and maturation (Chitu *et al*, 2016). In this study, we suggest that M-CSF is involved in autocrine loops in neuronal cells.

Based on these results, we hypothesized that M-CSF actions in neuronal cells could activate certain signaling pathways for antidepressant drugs. We discovered that Akt/GSK3β was phosphorylated by stimulation with M-CSF in neuronal cells. Shared with the mechanisms of conventional antidepressant drugs, our findings could be helpful to take less risk for developing novel therapeutics. Thus, these results indicate that the regulation of Akt/GSK3β pathways by M-CSF can be a strong candidate for the development of antidepressants.

In relation to BDNF signaling, we first verified that BDNF expression, as well as the phosphorylation of ERK1/2 and Akt/GSK3β was increased in neuronal cells both in $STAT3^{fl/fl}$;$LysM\text{-}Cre^{+/-}$ mice and in *in vitro* co-culture system in response to secreted M-CSF. M-CSF-induced ERK1/2 and Akt/GSK3β signaling pathways potentially work as the molecular mechanisms to regulate antidepressive-like behaviors. Many studies showed that the ERK1/2 and Akt/GSK3β signaling subsequently induce BDNF expression (Jope and Roh, 2006; Obata *et al*, 2003). BDNF production may also affect presynaptic neurotransmitter release rather than morphological changes of synapses. For this reason, it is important to note that M-CSF regulates antidepressant-targeting mediators and BDNF expression.

In order to examine which factors from microglia could increase the release of M-CSF from neurons, we analyzed the cytokine/chemokine profiles of microglia in the STAT3-deficient mouse model. The results showed that the expression of CCL2 was reduced in primary microglia isolated from $STAT3^{fl/fl}$;$LysM\text{-}Cre^{+/-}$ mice, as well as in STAT3-silenced BV2 cells from *in vitro* co-culture system (Supplementary Figure S9a–c). We assumed that CCL2 in microglia contributed to the increase of M-CSF in neurons. However, the following results indicated that CCL2 had no effects on the changes of M-CSF levels in neurons (Supplementary Figure S9d). Besides, the expression level of CCL2 had no differences between the brains of WT and $STAT3^{fl/fl}$;$LysM\text{-}Cre^{+/-}$ mice (Supplementary Figure S9e). These results indicate that CCL2 was not involved in the M-CSF production. Considering the modulation of M-CSF expression, alternatively, nuclear factor-κB (NF-κb) can be an intermediate factor in neuron–microglia interactions. It was reported that NF-κb was implicated in the transcriptional regulation of the M-CSF (Rajavashisth *et al*, 1995). Therefore, further studies are needed to investigate whether the STAT3-targeted factors in microglia regulate neuronal M-CSF production via NF-κb signaling.

When it comes to neuron-microglia cross-talk, cell-to-cell interactions have a pivotal role in intercellular communication. For example, CX3CR1/CX3CL1 signaling between microglia and neurons is involved in synaptic engulfment, resulted in synaptic elimination (Ueno *et al*, 2013; Zhan *et al*, 2014), and in the modulation of cytokine production and glutamatergic neurotransmission (Rogers *et al*, 2011; Scianni *et al*, 2013). CD200 and its receptor, CD200 receptor, also have critical roles in the interplay between neurons and microglia by controlling anti-inflammatory signaling and by maintaining them in a resting state (Hoek *et al*, 2000). Presumably, however, our data indicated that *de novo* mechanisms of neuron-microglia cross-talk would exist. Ablation of STAT3 in microglia did not alter the number of synaptic dendritic spines. The cytokine array and ELISA experiments also provided that M-CSF production occurs in neuronal cells but not IL-1β, TNF-α, IL-6, and IL-10.

As a novel antidepressant mechanism, rapid responses mainly occur through NMDA and AMPA receptor-mediated glutamatergic neurotransmission (Duman *et al*, 2012b). Our findings indicated that AMPA receptor-mediated synaptic activity was enhanced presynaptically without morphological changes in response to M-CSF. As previously mentioned, we determined the increase of ERK1/2 phosphorylation by stimulation of M-CSF. Regarding the ERK1/2 signaling pathways, the mEPSC frequency was decreased in the inhibition of phosphorylated ERK1/2 (Kushner *et al*, 2005). Thus, this implicated that M-CSF-induced ERK1/2 signaling could enhance the release probability of neurotransmitters. The findings that M-CSF enhanced glutamatergic

neurotransmission can help elucidate novel antidepressant mechanisms for a rapid-acting antidepressant response.

In conclusion, microglial STAT3 was essential for promoting M-CSF actions on synaptic transmission, which led to antidepressive-like behavior. We propose that ERK1/2 and Akt/GSK3β signaling pathways are involved in BDNF-dependent antidepressant behaviors *via* M-CSF secretion in neuronal cells. These findings may provide a novel therapeutic approach for alleviating major depressive disorders.

FUNDING AND DISCLOSURE

This study was supported by grants from the NRF funded by the Korea government (MISP; 2012R1A5A2A44671346 and MESF; 2012R1A2A2A01012897 and 2014R1A2A1A11053203 to SKY and 2012R1A5A2A44671346 to SK), the National R&D Program for Cancer Control, Ministry of Health & Welfare, Republic of Korea (0720540 to SKY and A120476 to SK), and Seoul National University Hospital (SNUH) Research Fund (3420130270 and 0320140100 to SKY). S-HK received a scholarship from the BK21-plus education program provided by the National Research Foundation of Korea (NRF). The authors declare no conflict of interest.

ACKNOWLEDGMENTS

We thank Jaerong Ahn, Haeri Lee, Joohan Woo, Seung-Eon Roh, Kyung-Jin Kim, and Chung-Hyun Cho for technical support and for reading the manuscript.

REFERENCES

Audet MC, Anisman H (2013). Interplay between pro-inflammatory cytokines and growth factors in depressive illnesses. *Front Cell Neurosci* **7**: 68.

Beurel E, Grieco SF, Jope RS (2015). Glycogen synthase kinase-3 (GSK3): regulation, actions, and diseases. *Pharmacol Ther* **148**: 114–131.

Brites D, Fernandes A (2015). Neuroinflammation and depression: microglia activation, extracellular microvesicles and microRNA dysregulation. *Front Cell Neurosci* **9**: 476.

Caldeira C, Oliveira AF, Cunha C, Vaz AR, Falcão AS, Fernandes A *et al* (2014). Microglia change from a reactive to an age-like phenotype with the time in culture. *Front Cell Neurosci* **8**: 152.

Chabot S, Williams G, Yong VW (1997). Microglial production of TNF-alpha is induced by activated T lymphocytes. Involvement of VLA-4 and inhibition by interferonbeta-1b. *J Clin Invest* **100**: 604–612.

Chen G, Huang L-D, Jiang Y-M, Manji HK (2000). The mood-stabilizing agent valproate inhibits the activity of glycogen synthase kinase-3. *J Neurochem* **72**: 1327–1330.

Chitu V, Gokhan Ş, Nandi S, Mehler MF, Stanley ER (2016). Emerging roles for CSF-1 receptor and its ligands in the nervous system. *Trends Neurosci* **39**: 378–393.

Chuang DM, Wang Z, Chiu CT (2011). GSK-3 as a target for lithium-induced neuroprotection against excitotoxicity in neuronal cultures and animal models of ischemic stroke. *Front Mol Neurosci* **4**: 15.

Cipriani A, Smith K, Burgess S, Carney S, Goodwin G, Geddes J (2006). Lithium versus antidepressants in the long-term treatment of unipolar affective disorder. *Cochrane Database Syst Rev* Cd003492.

Clausen BH, Lambertsen KL, Babcock AA, Holm TH, Dagnaes-Hansen F, Finsen B (2008). Interleukin-1beta and tumor necrosis factor-alpha are expressed by different subsets of microglia and macrophages after ischemic stroke in mice. *J Neuroinflam* **5**: 1–18.

Couch Y, Anthony DC, Dolgov O, Revischin A, Festoff B, Santos AI *et al* (2013). Microglial activation, increased TNF and SERT expression in the prefrontal cortex define stress-altered behaviour in mice susceptible to anhedonia. *Brain Behav Immun* **29**: 136–146.

Davis LL, Kabel D, Patel D, Choate AD, Foslien-Nash C, Gurguis GN *et al* (1996). Valproate as an antidepressant in major depressive disorder. *Psychopharmacol Bull* **32**: 647–652.

Domino ME, Burns BJ, Silva SG, Kratochvil CJ, Vitiello B, Reinecke MA *et al* (2008). Cost-effectiveness of treatments for adolescent depression: results from TADS. *Am J Psychiatry* **165**: 588–596.

Duman RS, Aghajanian GK (2012a). Synaptic dysfunction in depression: potential therapeutic targets. *Science* **338**: 68–72.

Duman RS, Aghajanian GK, Sanacora G, Krystal JH (2016). Synaptic plasticity and depression: new insights from stress and rapid-acting antidepressants. *Nat Med* **22**: 238–249.

Duman RS, Li N, Liu R-J, Duric V, Aghajanian G (2012b). Signaling pathways underlying the rapid antidepressant actions of ketamine. *Neuropharmacology* **62**: 35–41.

Dwivedi Y, Rizavi HS, Conley RR, Pandey GN (2005). ERK MAP kinase signaling in post-mortem brain of suicide subjects: differential regulation of upstream Raf kinases Raf-1 and B-Raf. *Mol Psychiatry* **11**: 86–98.

Dwivedi Y, Rizavi HS, Roberts RC, Conley RC, Tamminga CA, Pandey GN (2001). Reduced activation and expression of ERK1/2 MAP kinase in the post-mortem brain of depressed suicide subjects. *J Neurochem* **77**: 916–928.

Einat H, Yuan P, Gould TD, Li J, Du J, Zhang L *et al* (2003). The role of the extracellular signal-regulated kinase signaling pathway in mood modulation. *J Neurosci* **23**: 7311–7316.

El Kasmi KC, Holst J, Coffre M, Mielke L, de Pauw A, Lhocine N *et al* (2006). General nature of the STAT3-activated anti-inflammatory response. *J Immunol* **177**: 7880–7888.

Fang X, Yu SX, Lu Y, Bast RC, Woodgett JR, Mills GB (2000). Phosphorylation and inactivation of glycogen synthase kinase 3 by protein kinase A. *Proc Natl Acad Sci USA* **97**: 11960–11965.

Felger JC, Lotrich FE (2013). Inflammatory cytokines in depression: neurobiological mechanisms and therapeutic implications. *Neuroscience* **246**: 199–229.

Goodyer I, Dubicka B, Wilkinson P, Kelvin R, Roberts C, Byford S *et al* (2007). Selective serotonin reuptake inhibitors (SSRIs) and routine specialist care with and without cognitive behaviour therapy in adolescents with major depression: randomised controlled trial. *BMJ* **335**: 142.

Gourley SL, Wu FJ, Kiraly DD, Ploski JE, Kedves AT, Duman RS *et al* (2007). Regionally specific regulation of ERK MAP kinase in a model of antidepressant-sensitive chronic depression. *Biol Psychiatry* **63**: 353–359.

Hisaoka K, Takebayashi M, Tsuchioka M, Maeda N, Nakata Y, Yamawaki S (2007). Antidepressants increase glial cell line-derived neurotrophic factor production through monoamine-independent activation of protein tyrosine kinase and extracellular signal-regulated kinase in glial cells. *J Pharmacol Exp Ther* **321**: 148–157.

Hodes GE, Kana V, Menard C, Merad M, Russo SJ (2015). Neuroimmune mechanisms of depression. *Nat Neurosci* **18**: 1386–1393.

Hoek RM, Ruuls SR, Murphy CA, Wright GJ, Goddard R, Zurawski SM *et al* (2000). Down-regulation of the macrophage lineage through interaction with OX2 (CD200). *Science* **290**: 1768–1771.

Imai Y, Kohsaka S (2002). Intracellular signaling in M-CSF-induced microglia activation: Role of Iba1. *Glia* **40**: 164–174.

Jope RS, Roh M-S (2006). Glycogen synthase kinase-3 (GSK3) in psychiatric diseases and therapeutic interventions. *Curr Drug Targets* **7**: 1421–1434.

Kamat PK, Kalani A, Tyagi N (2014). Method and validation of synaptosomal preparation for isolation of synaptic membrane proteins from rat brain. *MethodsX* **1**: 102–107.

Karege F, Perroud N, Burkhardt S, Schwald M, Ballmann E, La Harpe R *et al* (2007). Alteration in kinase activity but not in protein levels of protein kinase B and glycogen synthase kinase-3beta in ventral prefrontal cortex of depressed suicide victims. *Biol Psychiatry* **61**: 240–245.

Khairova RA, Machado-Vieira R, Du J, Manji HK (2009). A potential role for pro-inflammatory cytokines in regulating synaptic plasticity in major depressive disorder. *Int J Neuropsychopharmacol* **12**: 561–578.

Kong E, Sucic S, Monje FJ, Reisinger SN, Savalli G, Diao W *et al* (2015). STAT3 controls IL6-dependent regulation of serotonin transporter function and depression-like behavior. *Scientific Reports* **5**: 9009.

Kreisel T, Frank MG, Licht T, Reshef R, Ben-Menachem-Zidon O, Baratta MV *et al* (2014). Dynamic microglial alterations underlie stress-induced depressive-like behavior and suppressed neurogenesis. *Mol Psychiatry* **19**: 699–709.

Kushner SA, Elgersma Y, Murphy GG, Jaarsma D, van Woerden GM, Hojjati MR *et al* (2005). Modulation of presynaptic plasticity and learning by the H-ras/extracellular signal-regulated kinase/synapsin I signaling pathway. *J Neurosci* **25**: 9721–9734.

Mori T, Miyamoto T, Yoshida H, Asakawa M, Kawasumi M, Kobayashi T *et al* (2011). IL-1beta and TNFalpha-initiated IL-6-STAT3 pathway is critical in mediating inflammatory cytokines and RANKL expression in inflammatory arthritis. *Int Immunol* **23**: 701–712.

Obata K, Yamanaka H, Dai Y, Tachibana T, Fukuoka T, Tokunaga A *et al* (2003). Differential activation of extracellular signal-regulated protein kinase in primary afferent neurons regulates brain-derived neurotrophic factor expression after peripheral inflammation and nerve injury. *J Neurosci* **23**: 4117–4126.

Page ME, Detke MJ, Dalvi A, Kirby LG, Lucki I (1999). Serotonergic mediation of the effects of fluoxetine, but not desipramine, in the rat forced swimming test. *Psychopharmacology* **147**: 162–167.

Park KH, Lee TH, Kim CW, Kim J (2013). Enhancement of CCL15 expression and monocyte adhesion to endothelial cells (ECs) after hypoxia/reoxygenation and induction of ICAM-1 expression by CCL15 via the JAK2/STAT3 pathway in ECs. *J Immunol* **190**: 6550–6558.

Rajavashisth TB, Yamada H, Mishra NK (1995). Transcriptional activation of the macrophage-colony stimulating factor gene by minimally modified LDL. *Arterioscler Thromb Vasc Biol* **15**: 1591.

Riazi K, Galic MA, Kuzmiski JB, Ho W, Sharkey KA, Pittman QJ (2008). Microglial activation and TNFα production mediate altered CNS excitability following peripheral inflammation. *Proc Natl Acad Sci USA* **105**: 17151–17156.

Riley JK, Takeda K, Akira S, Schreiber RD (1999). Interleukin-10 receptor signaling through the JAK-STAT pathway: requirement for two distinct receptor-derived signals for anti-inflammatory action. *J Biol Chem* **274**: 16513–16521.

Rogers JT, Morganti JM, Bachstetter AD, Hudson CE, Peters MM, Grimmig BA *et al* (2011). CX3CR1 deficiency leads to impairment of hippocampal cognitive function and synaptic plasticity. *J Neurosci* **31**: 16241–16250.

Schiepers OJ, Wichers MC, Maes M (2005). Cytokines and major depression. *Prog Neuropsychopharmacol Biol Psychiatry* **29**: 201–217.

Scianni M, Antonilli L, Chece G, Cristalli G, Di Castro MA, Limatola C *et al* (2013). Fractalkine (CX3CL1) enhances hippocampal N-methyl-d-aspartate receptor (NMDAR) function via d-serine and adenosine receptor type A2 (A2AR) activity. *J Neuroinflam* **10**: 876.

Steiner J, Walter M, Gos T, Guillemin GJ, Bernstein H-G, Sarnyai Z *et al* (2011). Severe depression is associated with increased microglial quinolinic acid in subregions of the anterior cingulate gyrus: evidence for an immune-modulated glutamatergic neurotransmission? *J Neuroinflam* **8**: 1–9.

Streit WJ, Mrak RE, Griffin WST (2004). Microglia and neuroinflammation: a pathological perspective. *J Neuroinflam* **1**: 1–4.

Strekalova T, Spanagel R, Bartsch D, Henn FA, Gass P (2004). Stress-induced anhedonia in mice is associated with deficits in forced swimming and exploration. *Neuropsychopharmacology* **29**: 2007–2017.

Tardito D, Perez J, Tiraboschi E, Musazzi L, Racagni G, Popoli M (2006). Signaling pathways regulating gene expression, neuroplasticity, and neurotrophic mechanisms in the action of antidepressants: a critical overview. *Pharmacol Rev* **58**: 115–134.

Ueno M, Fujita Y, Tanaka T, Nakamura Y, Kikuta J, Ishii M *et al* (2013). Layer V cortical neurons require microglial support for survival during postnatal development. *Nat Neurosci* **16**: 543–551.

Wake H, Moorhouse AJ, Miyamoto A, Nabekura J (2013). Microglia: actively surveying and shaping neuronal circuit structure and function. *Trends Neurosci* **36**: 209–217.

Zhan Y, Paolicelli RC, Sforazzini F, Weinhard L, Bolasco G, Pagani F *et al* (2014). Deficient neuron-microglia signaling results in impaired functional brain connectivity and social behavior. *Nat Neurosci* **17**: 400–406.

Supplementary Information accompanies the paper on the Neuropsychopharmacology website (http://www.nature.com/npp)